

Mass spectral characterization of secondary organic aerosol from urban cooking and vehicular sources

Wenfei Zhu¹, Song Guo^{1,2*}, Zirui Zhang¹, Hui Wang¹, Ying Yu¹, Zheng Chen¹, Ruizhe Shen¹, Rui Tan¹, Kai Song¹, Kefan Liu¹, Rongzhi Tang¹, Yi Liu¹, Shengrong Lou³, Yuanju Li¹, Wenbin Zhang⁴, Zhou Zhang⁴, Shijin Shuai⁴, Hongming Xu⁴, Shuangde Li⁵, Yunfa Chen⁵, Min Hu¹, Francesco Canonaco⁶, Andre. S. H. Prévôt⁶

¹ State Key Joint Laboratory of Environmental Simulation and Pollution Control, International Joint Laboratory for Regional Pollution Control, Ministry of Education (IJRC), College of Environmental Sciences and Engineering, Peking University, Beijing 100871, China P. R.

² Collaborative Innovation Center of Atmospheric Environment and Equipment Technology, Nanjing University of Information Science & Technology, Nanjing 210044, China P. R.

³ State Environmental Protection Key Laboratory of Formation of Urban Air Pollution Complex, Shanghai Academy of Environmental Sciences, Shanghai 200233, China P. R.

⁴ State Key Laboratory of Automotive Safety and Energy, Tsinghua University, Beijing 100084, China P. R.

⁵ State Key Laboratory of Multiphase Complex Systems, Institute of Process Engineering, Chinese Academy of Sciences, Beijing 100190, China P. R.

⁶ Laboratory of Atmospheric Chemistry, Paul Scherrer Institute (PSI), Villigen 5232, Switzerland

Corresponding authors:

*Song Guo – State Key Joint Laboratory of Environmental Simulation and Pollution Control, College of Environmental Sciences and Engineering, Peking University, Beijing 100871, China P. R.; Email: songguo@pku.edu.cn

Abstract In the present work, we conducted experiments of secondary organic aerosol (SOA) formation from urban cooking and vehicular sources to characterize the mass spectral features of primary organic aerosol (POA) and SOA using an high-resolution time-of-flight aerosol mass spectrometer (HR-ToF-AMS). Our results showed that the cooking styles have a greater impact on aged COA mass spectra than oxidation conditions. However, the oxidation conditions affect the aged HOA spectra more significantly than vehicle operating conditions. In our study, we use mass spectra similarity analysis and positive matrix factorization (PMF) analysis to establish the POA and SOA mass spectra of these two sources. These mass spectra are used

30 as source constraints in a multilinear engine (ME-2) model to apportion the OA sources in the atmosphere. Comparing with
31 the traditional ambient PMF results, the improved ME-2 model can better quantify the contribution of POA and SOA from
32 cooking and vehicular sources. Our work, for the first time, establishes the vehicle and cooking SOA source profiles, and can
33 be further used in the OA source apportionment in the ambient atmosphere.

36 **1. Introduction**

37 Organic aerosol (OA) is an important component of fine particulate matter and has significant
38 environmental and health effects, especially in urban areas (Guo et al., 2012; Guo et al., 2014; Ying et al.,
39 2020). Currently, real-time measurements of OA based on the aerosol mass spectrometer (AMS) has become
40 an effective way to explore OA characteristics in the field campaigns and laboratory studies (Canagaratna et
41 al., 2007; Ge et al., 2017; Hu et al., 2016a; Huang et al., 2011; Kim et al., 2017; Li et al., 2017; Sun et al.,
42 2016; Zhang et al., 2011). Applying positive matrix factorization (PMF) and a multilinear engine (ME-2)
43 (Paatero, 1999) to analyze the high-resolution mass spectrometry fragments, OA can be further identified as
44 primary organic aerosol (POA) and secondary organic aerosol (SOA). POA includes a kind of hydrocarbon-
45 like OA, (HOA), cooking (COA), and biomass burning (BBOA), which SOA includes low oxygenated OA
46 (LO-OOA) and more oxygenated OA (MO-OOA)(Canonaco et al., 2013; Elser et al., 2016; Qin et al., 2017;
47 Zhang et al., 2017a; Zhou et al., 2018). Many previous studies have been found that HOA is mainly associated
48 with vehicle-related emissions in the urban atmosphere (Hu et al., 2017; Xu et al., 2016; Zhang et al., 2017a).
49 Hereinafter, HOA will be referred to as the abbreviation for organic aerosol emitted by urban vehicles. As
50 lifestyle sources in urban, cooking and vehicular sources, that is COA and HOA mostly determine ambient
51 OA loadings. For example, primary cooking OA (COA) and vehicle exhaust OA (HOA) accounted for 10-35 %
52 and 6-26% of OA, respectively, in urban areas in China (He et al., 2011; Hu et al., 2017; Sun et al., 2010; Sun
53 et al., 2014; Sun et al., 2018; Wang et al., 2016; Xu et al., 2016; Zhang et al., 2014).

Besides the contribution to POA, many studies have found that cooking and vehicular sources may also emit a large number of volatile organic compounds (VOCs) (Gentner et al., 2009; Katragadda et al., 2010; Klein et al., 2016), semi-volatile organic compounds (SVOCs), and intermediate volatile organic compounds (IVOCs) ($\geq C_{13}$ n-alkanes and fatty acids) (Louvaris et al., 2017; Schauer et al., 2002; Tang et al., 2021), which may also play important roles in SOA formation (Wang et al., 2021; Yu et al., 2021). However, based on collocated AMS measurements and factor analysis results, the SOA formed by vehicle and cooking sources cannot be effectively resolved from the total SOA due to the lack of secondary mass spectral profiles. The POA mass spectral profiles based on AMS including HOA (Collier et al., 2015), BBOA (Alfarra et al., 2007; He et al., 2010; Xu et al., 2020), and COA (He et al., 2010; Liu et al., 2017; Mohr et al., 2012; Xu et al., 2020) have been fully explored in laboratory studies and applied as constraint factors into the ME-2 model in the ambient air. Some studies have made it possible to quantify biogenic secondary aerosol products of a single precursor, such as isoprene oxidation products (IEPOX) (Budisulistiorini et al., 2013; Hu et al., 2016b), and have been extended to the urban atmosphere to obtain an IEPOX-SOA factor via PMF analysis of OA spectra (Zhang et al., 2017b). Although several studies explored the mass spectral characteristics of SOA from cooking and vehicular sources, i.e., heated cooking oils, gasoline motors, and diesel engines (Kaltsonoudis et al., 2017; Kroll et al., 2012; Liu et al., 2018; Presto et al., 2014), the spectral profiles of cooking SOA under actual cooking conditions and vehicle SOA under different emission conditions are still uncertain. Besides, to date, studies that used ME-2 for a better anthropogenic SOA source apportionment by inputting their SOA spectra as constraints remain scarce. Therefore, the mass spectra of SOA from abundant cooking and vehicular sources are urgent to characterize for conducting to acquire a better source apportionment of SOA.

In this study, cooking and vehicle experiments were carried out to investigate the variation in POA and SOA spectra profiles emitted from vehicle emissions under different running conditions, and Chinese cooking emissions under different cooking styles using high-resolution time-of-flight AMS (HR-ToF-AMS). The mass

spectral characterizations of POA and SOA from cooking and vehicle emissions were intercompared, and their changes in some indicated ionic fragments were elucidated. Besides, we verified the mass spectral profiles by applying POA and SOA profiles to ME-2 for source apportionment of OA in the winter observation with various primary emissions and the summer observation with high oxidation conditions.

2. Materials and Methods

2.1 Simulation of POA emission and SOA formation from cooking and vehicular sources.

For cooking, we prepared four dishes including deep-frying chicken, shallow-frying tofu, stir-frying cabbage, and Kung Pao chicken. The total cooking time for each experiment ranged from 40 to 66 min, which was almost related to the features of each dish (**Table S1**). Each dish was continuously carried out 8 times in parallel during the cooking process until the closed kitchen was full of fumes. The fumes produced by cooking were introduced through the pipeline from the kitchen into the Gothenburg Potential Aerosol Mass (Go: PAM) reactor (Li et al., 2019) in the laboratory after being diluted 8 times by a Dekati Dilutor (e-Diluter, Dekati Ltd., Finland). Heat insulation cotton was wrapped around the sampling pipelines to prevent fumes from condensing on the wall of the pipe. We considered the emissions sampled after Go: PAM without OH radical as primary emissions, and those monitoring after Go: PAM with given OH radicals as secondary formation. The sampling time ranged from 58 to 90 min. In addition, the background blank groups and the dilution gas blank groups were separately completed using boiling water and dilution gas, according to the same steps as experimental groups. More information on the experimental setup of cooking simulations has been given in Zhang et al., 2020.

For vehicle, experiments were performed by using a Gasoline direct engine (GDI) with a commercial China V gasoline fuel (Emission: 998cc; Maximum power: 100KW 6000rpm; Peak torque: 205Nm 2000-3000rpm). Vehicle operating under real-life conditions were dynamic rotating speed-torque combination. For example, the combination of 1500 rpm rotating speed and 16Nm torque and 2000rpm rotating speed and

16Nm torque for the engine in this study reflect the realistic vehicle speed of 20km/h and 40km/h, respectively. Five running conditions covering different speeds and torques, including 1500rpm_16Nm, 1750rpm_16Nm, 2000rpm_16Nm, 2000rpm_32Nm, and 2000rpm_40Nm, were used to characterize their POA and SOA mass spectra in this study. Once the engine warmed up, it continued to work under one running condition. After the three-way catalytic system, the exhaust from the engine tailpipe was diluted 30 times by the same dilution system for the cooking experiment. Then the diluted exhaust entered the Go: PAM through the stainless pipe wrapped by heat insulation cotton. For each running condition, five parallel experiments were conducted (**Table S2**). The sampling time was about 60 min for each experiment.

Go: PAM reactor consists of quartz tube that is 100 cm long and 9.6 cm in diameter, as described in Watne et al., 2018. The OH radicals in Go: PAM reactor is generated by the photolysis of ozone and the reaction in the presence of water vapor. We adjusted input ozone concentrations ranging from ~0 to ~6.5 ppm and ~0 to ~4.0 ppm to change the OH radicals in the Go: PAM for vehicle and cooking experiments, respectively. The temperature, relative humidity, and the sampling residence time in Go: PAM for vehicle and cooking experiments were documented in the supplement material (**Table S3**).

2.2 Instrumentation and data analysis.

The design drawing on vehicle and cooking experiments is presented in **Figure S1**. Two scanning mobility particle sizers (SMPS; TSI Incorporation, USA) were set at the inlet and outlet of Go: PAM to correct the wall loss (Zhang et al., 2020). The size distribution and number concentration of particles were scanned every 2 (cooking) - 5 min (vehicle) before and after Go: PAM for cooking and vehicle experiment, respectively. The mass concentrations of non-refractory submicron aerosol (NR-PM₁), and high-resolution ions fragments of OA were recorded by HR-ToF-AMS (Aerodyne Research Incorporation, USA), synchronize with SMPS.

Before and after the two experiments, the ionization efficiency (IE) of HR-ToF-AMS was calibrated by applying 300 nm mono-dispersed ammonium nitrate particles synchronization with SMPS. The collection

123 efficiency (CE) was obtained from comparing AMS and synchronous SMPS real-time measurement of particle
124 mass concentrations at the outlet of Go: PAM. Besides, the real-time measurements of CO₂ concentrations
125 (Model 410i, Thermo Electron Corporation, USA) were used to correct the influence of CO₂ on OA ion
126 fragments, refer to (Canagaratna et al., 2015). Other gas phase measurements included carbon monoxide (CO,
127 Thermo, Model 48i TL), NO_x (Thermo, Model 42i TL), and SO₂ (Thermo, Model 42i TL).

128 The mass concentration, size distribution, and the ion-speciated mass spectra of NR-PM₁ species were
129 analyzed using the HR-ToF-AMS standard data analysis software (SQUIRREL version 1.57 and PIKA version
130 1.16). The elemental compositions (O/C, H/C, N/C, and OM/OC) were estimated by the “improved-ambient”
131 updated method (Canagaratna et al., 2015). The OH exposure and equivalent photochemical age (EPA) were
132 calculated by off-line methods according to SO₂ decay shown in Zhang et al., 2020, which were validated by
133 a flow reactor exposure estimator using measured concentrations of reactive compounds such as VOCs, CO,
134 and NO_x (Peng et al., 2016). The OH exposure and photochemical age for all conditions in cooking and vehicle
135 experiments were listed in **Table S3**.

136 **2.3 OA source apportionment**

137 The PMF model can describe the variability of a multivariate database as a linear combination of static
138 factor profiles and their corresponding time series (Huang et al., 2020; Wang et al., 2017; Zhu et al., 2018). In
139 this study, we used the Igor-based PMF model with PMF2.exe algorithm (Paatero and Hopke, 2003) and the
140 PMF Evaluation Toolkit version 2.08D (Ulbrich et al., 2009) to split POA and SOA factors from cooking and
141 vehicle aged OA. The PMF model was also used to identify the source of OA for ambient atmosphere during
142 the summer and winter observations of Shanghai, following the procedure presented in the literature (Hu et
143 al., 2016a; Zhang et al., 2011), as described in section 3.3. In contrast to an unconstrained PMF analysis, ME-
144 2 algorithm allows the user to add prior information (e.g., source profiles) into the model to constrain the
145 matrix rotation and separated the mixed solution. In this study, we adopted the toolkit SoFi (Source Finder)

146 with an a-value approach to perform organic HR-AMS datasets collected in Shanghai. The a-value can vary
147 between 0 and 1, which is the extent to which the output profiles can vary from the model inputs. The a-value
148 test was performed following the technical guidelines presented in Crippa et al., 2014. The reference mass
149 spectral profiles that constrained in ME-2 analysis were derived from lab-based primary and secondary
150 cooking and vehicular factors of this study. Details of the algorithm could refer to previous studies (Canonaco
151 et al., 2013; Huang et al., 2020; Reyes-Villegas et al., 2016).

152 **2.4 Mass spectra similarity analysis.**

153 In this study, the angle θ was used to evaluate the correlation between the two AMS mass spectra features.

154 The angle θ between the two AMS mass spectra (MSa, MSb) is given by:

$$155 \cos \theta = \frac{MSaMSb}{|MSa||MSb|}$$

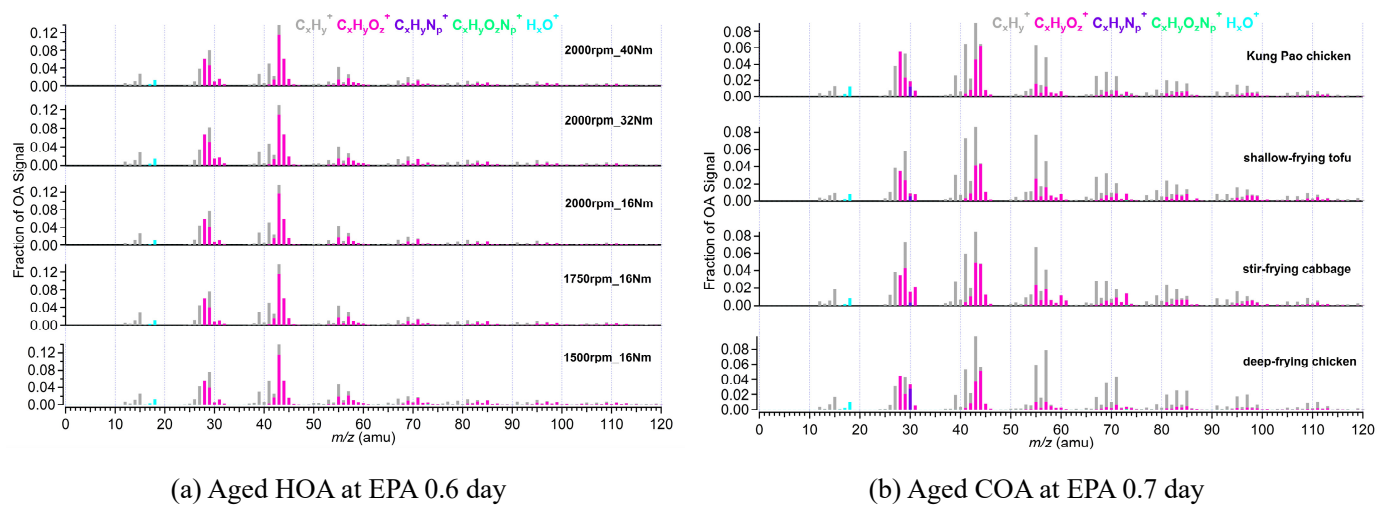
156 The θ angle between two mass spectra is 0-5, 5-10, 10-15, 15-30, and > 30 , which means excellent
157 consistency, good consistency, many similarities, limited similarities, and poor consistency, respectively
158 (Kaltsonoudis et al., 2017; Kostenidou et al., 2009).

159 **3. Results and Discussion**

160 **3.1 Mass spectra of POA and aged OA from the cooking and vehicular sources.**

161 **Fig.1a** shows the mass spectra of aged HOA under different vehicle running conditions when EPA was
162 0.6 days. The mass spectra of aged HOA emission from different vehicle running conditions under other
163 various oxidation degrees are included in **Fig.S2**. All the aged HOA spectral profiles from different vehicle
164 running conditions showed a similar pattern, and the θ angles among the mass spectra of aged HOA were less
165 than 10° at EPA 0.6 days (**Table 1**), suggesting a little difference between the mass spectra. The mass spectra
166 of aged HOA at 0.6 days were dominated by the ion series of $C_nH^{+}_{2n+1}$ (m/z 29, 43, 57, 71, 85...) and $C_nH_{2n-1}^{+}$
167 (m/z 41, 55, 69, 83...), resulting from less oxidized components such as saturated alkanes, alkenes. As the
168 highest proportion of ion fragments, m/z 43 and 29 consisted of oxygen-containing ions like CHO^+ and

169 $C_2H_3O^+$, respectively, whose fractions were much larger than the hydrocarbon-like ion fragments at the same
170 mass integers. Besides, there were also abundant tracer ion fragments for SOA (m/z 28 and m/z 44).



171
172 (a) Aged HOA at EPA 0.6 day (b) Aged COA at EPA 0.7 day
173 Fig. 1. (a) The mass spectra of aged HOA emission from different vehicle running conditions at EPA 0.6 day; (b) The mass
174 spectra of aged COA from four Chinese dishes at EPA 0.7 day. Five running conditions cover different speeds and torques,
175 including 1500rpm_16Nm, 1750rpm_16Nm, 2000rpm_16Nm, 2000rpm_32Nm, and 2000rpm_40Nm. Four dishes include
176 deep-frying chicken, shallow-frying tofu, stir-frying cabbage, and Kung Pao chicken.

171

172 The mass spectra of aged COA at 0.7 days of EPA are presented in **Fig.1b**. Detailed mass spectra of aged
173 COA under other various oxidation degrees are included in **Fig.S3**. The similarity of aged COA among
174 different types of cooking was greater than that of aged HOA among different running conditions when the
175 EPA was at the same level. Except for the θ angles of deep-frying chicken vs stir-frying cabbage (21°), and
176 deep-frying chicken vs shallow-frying tofu (19°), the θ angles among other aged COA at EPA 0.7 day exhibited
177 good agreement ($\theta < 15^\circ$) in mass spectra (**Table 1**). The mass spectra of cooking were dominated by the similar
178 ion series as those of vehicle, which were mostly m/z 28, m/z 29, m/z 41, m/z 43, m/z 44, m/z 55, m/z 57, m/z
179 67, and m/z 69. However, the major mass spectral differences between cooking and vehicle were the
180 abundance of m/z 41 and the ratio of oxygen-containing ions to hydrocarbon ions ($C_xH_yO_z^+/C_xH_y^+$). The four
181 Chinese dishes had prominent peaks at m/z 41, m/z 43, and m/z 55 (generated from $C_3H_5^+$ and $C_3H_7^+$, $C_4H_7^+$)
182 which was qualitatively consistent with mass spectra of primary COA in other studies (Xu et al., 2020). As
183 described by He et al., 2010, the most abundant ion fragments at m/z 41 and m/z 55 from primary Chinese

184 cooking emissions associated with frying are resulting from unsaturated fatty acids

185
186 Table 1 The θ angles among the mass spectra of (a) aged HOA at EPA 0.6 day and (b) aged COA at EPA 0.7 day

(a) θ angles	1500rpm_16Nm	1750rpm_16Nm	2000rpm_16Nm	2000rpm_32Nm	2000rpm_40Nm
1500rpm_16Nm	0	3	3	8	4
1750 rpm_16 Nm		0	0.1	5	3
2000 rpm_16 Nm			0	5	3
2000 rpm_32 Nm				0	4
2000 rpm_40 Nm					0

(b) θ angles	deep-frying chicken	stir-frying cabbage	shallow-frying tofu	Kung Pao chicken
deep-frying chicken	0	21	19	14
stir-frying cabbage		0	10	13
shallow-frying tofu			0	12
Kung Pao chicken				0

187
188
189 **Fig.2a** shows the mass spectra of aged HOA oxidation at different OH exposures under the same vehicle
190 running condition (2000rpm, 16Nm). The changes in mass spectra of aged HOA under different conditions
191 are provided in **Fig.S4**. It was worth noting that the source characteristics of vehicle POA were uncertain due
192 to its low concentration emitted from the engine in this study (**Table S4**). A related study has found that the
193 POA factor from vehicle emissions is similar to the HOA factor derived from environmental datasets (Presto
194 et al., 2014). Therefore, we used the average HOA spectrum derived from unconstrained PMF analysis based
195 on the ambient observations of Shanghai, Beijing, Dezhou, Shenzhen in China as an alternative to the mass
196 spectrum of vehicle POA, as shown in **Fig.2a** and **Fig.S4**. Detail observation information of Shanghai, Dezhou,
197 and Shenzhen referred to Zhu et al., 2021a. The observations in Beijing have been given in Hu et al., 2017.
198 The HOA spectrum was similar to that reported in Ng et al., 2011, which has been widely used as traffic
199 emission profiles. As the oxidation degree increased, the ion fragments varied similarly with hydrocarbon-like

ion fragments decreasing. The mass spectra at 2.9 days and 4.1 days had very similar patterns with the most abundant signals at m/z 28 and 44, respectively (**Fig.2** and **Fig.S4**), which showed good consistency with the mass spectra of MO-OOA resolved from ambient datasets ($\theta = 14^\circ$; compared with MO-OOA obtained during the spring observations in Ng et al., 2011; Zhu et al., 2021b). When EPA was 1.7 days, there were different mass spectra patterns, with dominant signals at m/z 28 and m/z 44, yet contained a large signal at m/z 43, many similarities with the spectra of the ambient LO-OOA (**Fig.2** and **Fig.S4**) (Hu et al., 2017; Zhu et al., 2021b). Oxidation degrees greatly affected the similarity of mass spectra between POA and those of aged HOA. The mass spectra profile of HOA_ambient displayed poor agreement ($\theta > 30^\circ$) with all aged HOA spectra profiles (**Tables S7**). Besides, the mass spectra under the low oxidation degree (EPA was 0.6 day) was also poorly correlated with those mass spectra under the high oxidation degree (EPA were 2.9 and 4.1 days) (**Table S7**).

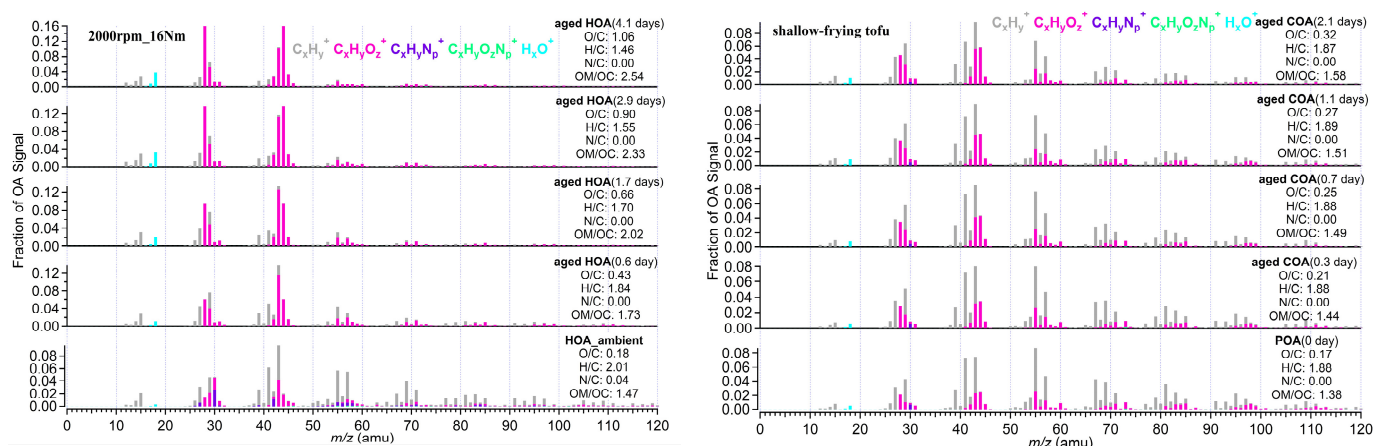


Fig.2. (a) The mass spectra of HOA and aged HOA oxidation under four different OH exposure at the same running condition (2000rpm, 16Nm). (b) The mass spectra of primary COA and aged COA oxidation of different OH exposure for shallow-frying tofu. The EPA was obtained from off-line methods according to SO_2 decay shown in Table S3. The elemental compositions were estimated by the “improved-ambient” updated method (Canagaratna et al., 2015).

The mass spectra of primary COA and aged COA showed great inter-correlations ($\theta < 15^\circ$), which were smaller than that of vehicle OA (**Table S8**). The spectra of aged COA derived herein displayed good consistency with those from cooking oils (Liu et al., 2018) (**Fig.2b** and **Fig.S5**). It should be noted that the fractions of m/z 28 and m/z 44 signals in aged COA were lower than those of aged HOA at the similar EPA.

216 In addition, the aged COA had more hydrocarbon-like ions at the same mass integers than aged HOA.

217 All the above results imply that oxidation condition drives the variabilities in mass spectra of the vehicle
218 OA. In contrast, cooking styles instead of oxidation conditions significantly affected the mass spectra of
219 cooking OA. Here we concluded some possible explanations for these results. On one hand, under the same
220 oxidation conditions and different emission conditions, the similarity among the mass spectra of vehicles was
221 larger than that of cooking, which may be related to their precursors. Some studies have shown that the species
222 and the proportion of gaseous organic matter emitted by different dishes are quite different (Wang et al., 2018).
223 As described in the literature, alkanes and oxygenated volatile organic compounds (O-VOCs) contributed to
224 over 97% of the total VOCs for fried food, and O-VOCs were the dominant contributors for Sichuan and
225 Hunan cuisine where stir-frying is common (Wang et al., 2018). Different gaseous precursors cause
226 distinctions in the particle phase SOA formation, which is reflected in the variations of AMS ion fragments
227 between four dishes in our study. Compared to cooking, the precursors from vehicles are mainly hydrocarbons,
228 and the difference in emissions under different running conditions is inapparent (Robinson et al., 2007). On
229 the other hand, under the same emission conditions and different oxidation conditions, the similarity among
230 the mass spectra of cooking sources is larger than that of vehicle sources, likely due to the oxidation pathway
231 of precursors. As mentioned above, O-VOCs are important precursors of cooking sources, and their oxidation
232 mechanisms are mostly alcohol/peroxide substitution process. This conclusion was proved by a Van Krevelen
233 diagram, showing that the cooking data gather around the slope of approximately -0.1 (Zhang et al., 2020), in
234 agreement with that of heated oils OA (Liu et al., 2018). However, for vehicles, with the increase of oxidation
235 degrees, the reaction pathways of hydrocarbon precursors varied diversely. In Van Krevelen space, the vehicle
236 data fell along a line with a slope of -0.5 (**Fig.S6**), indicating oxidation processes involving the addition of
237 both carboxylic acid and alcohol or peroxide functional groups without fragmentation and/or the addition of
238 carboxylic acid functional groups with fragmentation.

3.2 Identification of the cooking and vehicular sources SOA mass spectra.

Although the f_{44} (proportion of m/z 44 in OA) of aged COA raised from 0.03 to 0.08 with oxidation increasing (**Fig.2b** and **Fig.S5**), the high abundance of m/z 41, 55, and 57 in aged COA mass spectra for four dishes may be a sign that aged COA identified in this study is a mixture of POA and SOA. PMF analysis was performed on the high-resolution mass spectra to split SOA and POA factors from integrated primary COA and aged COA under each dish. Similarly, the same PMF procedure was also applied for vehicle aged datasets for each running condition. The choice of the PMF solution can be found in the supplement material (**Fig.S7-S10** and **Table S9-S10**; taken stir-frying cabbage for cooking, and 2000rpm_32Nm for vehicle as an example).

Some ions like m/z 41, 55, 57, 43, 28, and 44 are typically used as tracers of OOA, COA, HOA, LO-OOA, and MO-OOA. **Fig.3** shows the high-resolution mass spectra of POA and SOA from four Chinese dishes and five vehicle running conditions. The cooking PMF POA of four Chinese dishes all showed obvious hydrocarbon-like signals at m/z 41, 43, 55, 57, 67, and 69 with ion fragments of $C_3H_5^+$, $C_3H_7^+$, $C_4H_7^+$, $C_4H_9^+$, $C_5H_7^+$, and $C_5H_9^+$, respectively. The fraction of m/z 41 in cooking POA ranged from 0.051 to 0.069. The prominent fraction of m/z 43 ($f_{43}=0.068\sim 0.083$), 55 ($f_{55}=0.064\sim 0.084$), 57 ($f_{57}=0.041\sim 0.097$), 67 ($f_{67}=0.021\sim 0.40$), 69 ($f_{69}=0.034\sim 0.049$) were observed (Table S10). For mass spectra of cooking PMF SOA, the oxidized ion fragments had higher signals than those of hydrocarbon-like ion fragments. The dominant signals existed at m/z 28 ($f_{28}=0.045\sim 0.068$), 29 ($f_{29}=0.048\sim 0.080$), 41 ($f_{41}=0.050\sim 0.068$), 43 ($f_{43}=0.087\sim 0.103$), 44 ($f_{44}=0.058\sim 0.080$), 55 ($f_{55}=0.050\sim 0.064$) (Table S11).

Different from the cooking, two-vehicle PMF SOA factors were derived from aged HOA, rather than integrated primary HOA and aged HOA datasets due to the low primary HOA emission (**Table S4**), as described in sect. 3.1. Unfortunately, vehicle PMF POA factor cannot be separated from aged HOA due to higher OH exposure. According to different O/C ratios, they were considered to be low oxidized vehicle SOA (LO-SOA) and more oxidized vehicle SOA (MO-SOA). As indicated in **Fig.3** and **Table S13**, the prominent

262 m/z 28 (average $f_{28}=0.045$), 41 (average $f_{41}=0.046$), 43 (average $f_{43}=0.158$), 44 (average $f_{44}=0.054$), 55
 263 (average $f_{55}=0.039$), 57 (average $f_{57}=0.027$) of vehicle PMF LO-SOA were comparable with those of cooking
 264 PMF SOA. The fraction of m/z 43 of vehicle PMF LO-SOA was higher than that in cooking SOA by a factor
 265 of 2, which may be caused by the inability to separate vehicle PMF POA factor in the PMF analysis. The
 266 abundant m/z 28 and 44 (mainly generated from CO_2^+) are widely used as the ambient MO-OOA markers
 267 (Sun et al., 2018; Xu et al., 2017). We observed high fractions of m/z 28 ($f_{28}=0.110\sim 0.214$) and m/z 44
 268 ($f_{44}=0.121\sim 0.224$) in vehicle PMF MO-SOA (Table S13) and high O/C ratios (0.88~1.33), which were much
 269 higher than those of vehicle PMF LO-SOA (O/C=0.37~0.53) and cooking SOA (O/C=0.29~0.41).

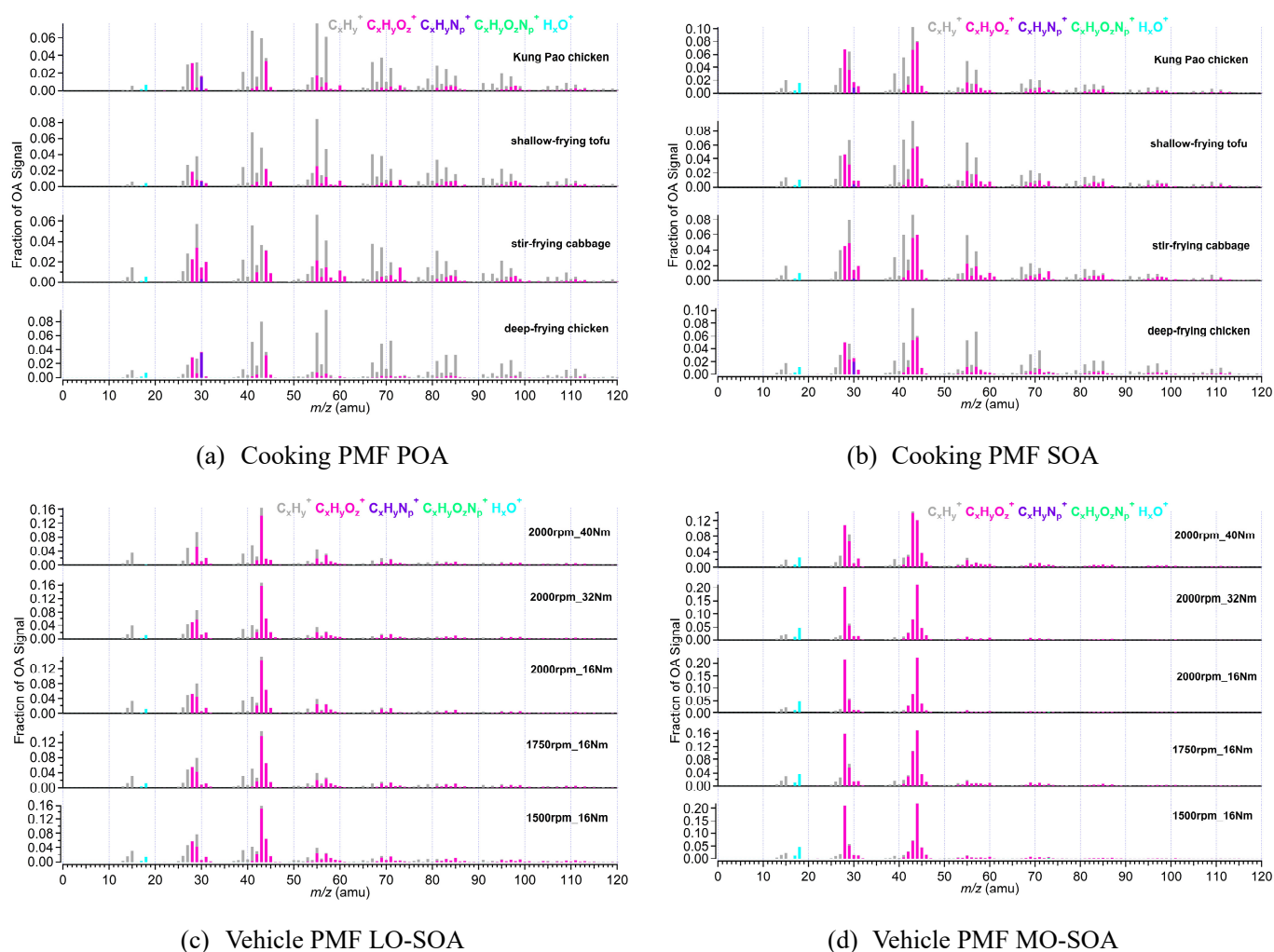


Fig.3. The mass spectra of PMF POA and SOA from vehicle and cooking. PMF analysis was performed on the high-resolution mass spectra to split two factors (cooking POA and SOA) from aged COA and two SOA factors (vehicle LO-SOA and MO-SOA) from aged HOA, respectively.

270

271 Similarly, for the resolved SOA factors, the correlation of mass spectra among cooking groups under
272 different cooking methods ($\theta = 8\sim 21^\circ$) was worse than that of vehicle groups (vehicle PMF LO-SOA; $\theta =$
273 $3\sim 19^\circ$) under different running conditions (**Table S15** and **Table S17**). The mass spectra of the PMF POA
274 factors for deep-frying chicken exhibited poor agreement with those of stir-frying cabbage, Kung Pao chicken,
275 and shallow-frying tofu (**Table S16**). In addition, we also found that the θ angles between vehicle PMF LO-
276 SOA and vehicle PMF MO-SOA under five GDI running conditions were ranged from 36° to 50° (**Fig.S11**),
277 indicating that the mass spectra profiles of vehicle PMF LO-SOA are poor consistency with those of vehicle
278 PMF MO-SOA, consistent with the changes in the mass spectra characteristics of vehicles, under the same
279 emission conditions and different oxidation conditions. Our results suggest that it is necessary to consider the
280 cooking styles when constraining cooking and atmospheric oxidation conditions when constraining vehicle
281 factors.

282 **3.3 Application of established POA and SOA profile in ambient OA source apportionment.**

283 The POA and SOA of the cooking as the primary and secondary spectrum constraints for ME-2 were
284 obtained by averaging the high-resolution mass spectra datasets of the four dishes, which were identified from
285 aged COA using the PMF model. Similarly, combining different GDI running conditions, the averaged vehicle
286 LO-SOA and vehicle MO-SOA which were resolved based on aged HOA by using the PMF model were used
287 as the inputting mass spectra profiles of vehicles for ME-2. The mass spectral profiles for cooking and vehicle
288 as constraints in the ME-2 model are shown in **Fig.S12**.

289 The θ angles between the mass spectral profiles from urban cooking and vehicular sources and ambient
290 PMF-resolved factors were calculated and summarized in **Fig.4** and **Table S19**. The AMS mass spectra of
291 ambient factors were obtained and averaged in Shanghai, Dezhou, Beijing, and Shenzhen in China (Hu et al.,
292 2017; Zhu et al., 2021a). The θ angles among ambient COA, HOA, LO-OOA, and MO-OOA factors and the
293 cooking POA, SOA, and the vehicle LO-SOA, vehicle MO-SOA were ranged from 18° to 52° (**Fig.4**),

294 suggesting that the cooking POA, cooking SOA, and the vehicle LO-SOA, vehicle MO-SOA can be used as
295 source constraints for ME-2 in ambient air.

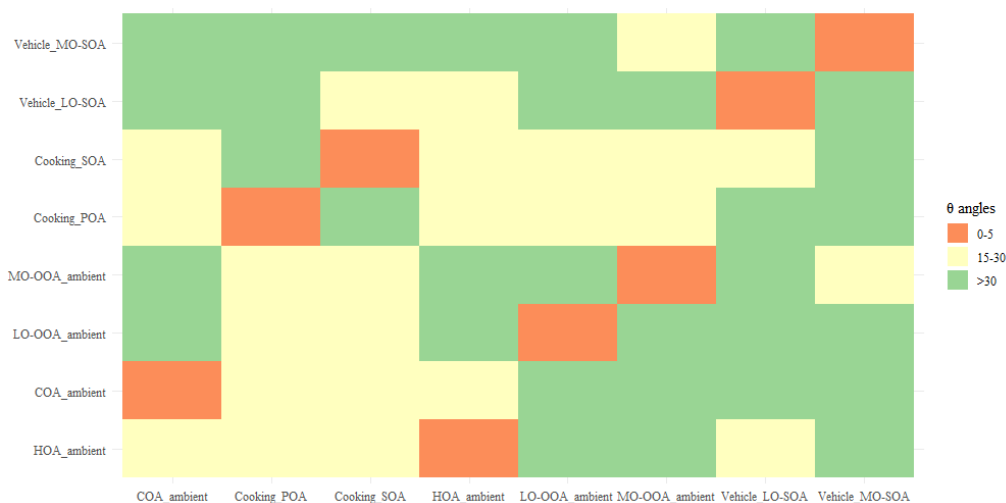


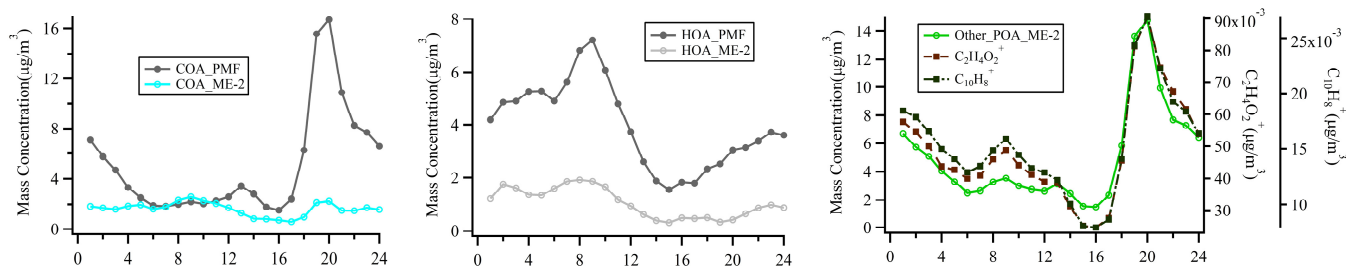
Fig.4. The θ angles between ambient COA, HOA, LO-OOA, and MO-OOA factors and the cooking PMF POA, SOA, and the vehicle LO-SOA, MO-SOA. The θ angle between two mass spectra is 0-5, 5-10, 10-15, 15-30, and > 30 indicates excellent consistency, good consistency, many similarities, limited similarities, and poor consistency, respectively. The ambient COA, HOA, LO-OOA, and MO-OOA factors were averaged the resolved factors which performed on Shanghai, Dezhou, Beijing, and Shenzhen datasets (Hu et al., 2017; Zhu et al., 2021a).

296

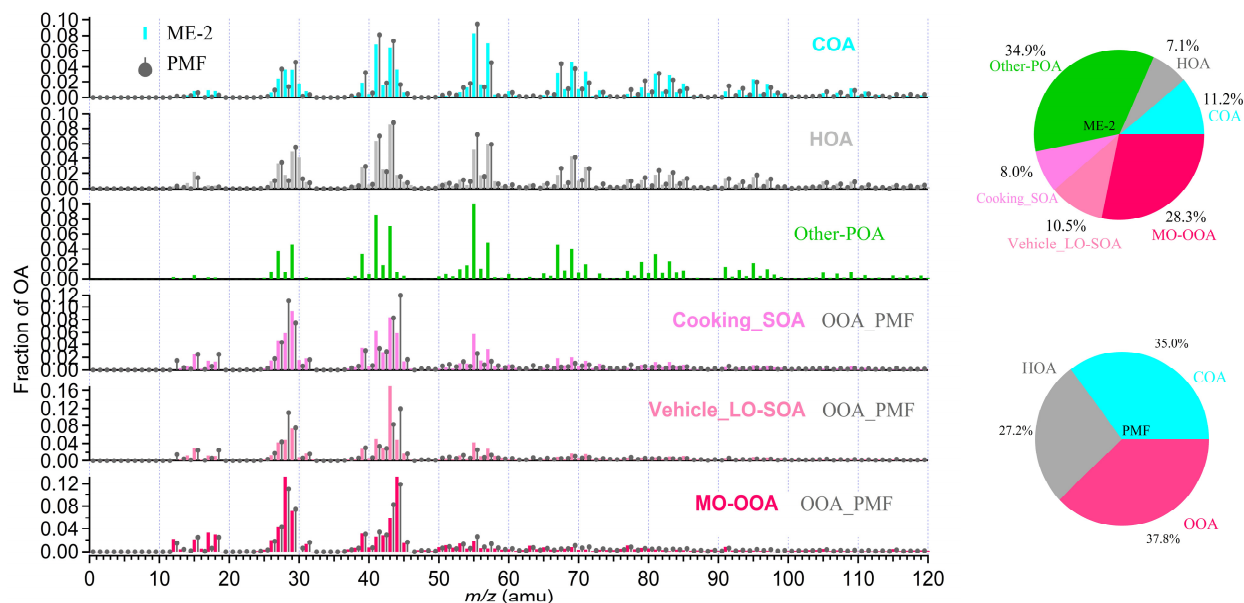
297 Considering the actual oxidation conditions, that is the concentration of OH radicals, and the lacking
298 vehicle POA due to its low emission (**Table S4**), and the SOA spectra constraining reasonably, the cooking
299 POA, cooking SOA, vehicle LO-SOA, and ambient HOA (instead of vehicle POA; derived from Beijing,
300 Shenzhen, Dezhou, Shanghai ambient measurements) was finally selected as the input source spectra of ME-
301 2. We further demonstrated the feasibility of input primary and secondary mass spectra for OA source
302 apportionment in two field campaigns at the urban site of Shanghai in summer and winter. The ambient
303 measurements in Shanghai were taken in situ at the same location as Zhu et al., 2021a, i.e., Shanghai Academy
304 of Environmental Sciences (31.10°N,121.25°E), a typical urban site in the Yangtze River Delta region from
305 23 August to 5 September 2016, and from 28 November 2016 to 12 December 2017 with HR-ToF-AMS at 4
306 min time resolution. For the tracers described below, the mass concentration of chemical compositions e.g.,
307 sulfate, nitrate, and ion-specified fragment were detected by HR-ToF-AMS, as shown in Zhu et al., 2021b.

308 The detail measurements of black carbon (BC) and nitrogen oxides (NO_x) can also be found in Zhu et al.,
309 2021b. In general, the ME-2 source analysis was performed by constraining two primary OA factors (the
310 cooking POA, HOA) and two secondary OA factors (the cooking SOA, the vehicle LO-SOA) with the fixed
311 a-value of 0.1 for HOA, 0.2 for cooking POA, 0.4 for vehicle LO-SOA and cooking SOA based on the same
312 ambient OA datasets of the summer and winter observations in Shanghai. In ME-2 solutions from 1 to 7 factors,
313 we found the solution of 6 factors (i.e., COA, HOA, Other-POA, Cooking SOA, Vehicle LO-SOA) was most
314 interpretable for the wintertime observations. For the 5 factors solution, in addition to the constraint four
315 factors, factor 5 appeared to be mixed primary and secondary features. However, Other-POA split into two
316 factors with similar profiles in seven factors solution (**Fig.S13**). Source apportionment on OA datasets by
317 using the unconstrained PMF model was also examined to compare with ME-2 analysis. The choice for the
318 optimal solution for the PMF model was presented in the supporting information (**Fig.S14-S16** and **Table**
319 **S20-S21**). Ambient PMF-resolved OA factors included POA factors (i.e., HOA, COA), and SOA factors i.e.,
320 OOA (oxygenated OA) in the winter observations in Shanghai, on average accounting for 27%, 35%, and 38%
321 of OA mass. OOA resolved by PMF model did not separate into two types of OOAs including LO-OOA and
322 MO-OOA. Besides, we observed that HOA and COA profiles (provided via PMF during the wintertime)
323 contained high signals at the biomass burning tracer ion (m/z 73), and m/z 91 (PAH-related m/z), indicating
324 that the mixing among HOA, COA, and other source emissions (e.g., BBOA) (**Fig.5**).

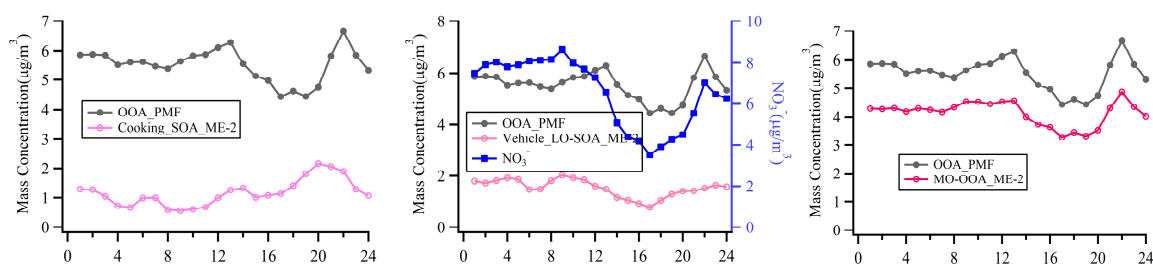
328



329



330



331

Fig.5. The comparison of the mass spectra, the diurnal variation, and fraction between ME-2 and PMF resolved factors during the wintertime in Shanghai. The black lines in the spectra and diurnal pattern are the results of PMF analysis of the actual atmosphere in Shanghai winter. The others correspond to the ME-2 source analysis results by using two primary OA factors (the cooking POA, ambient HOA) and two secondary OA factors (the cooking SOA, the vehicle LO-SOA) as constraints based on the same ambient OA datasets as the PMF model during the winter observations of Shanghai. Note that in the mass spectra and daily patterns, the OOA_PMf factors which compared with vehicle LO-SOA and Cooking SOA respectively are the same, rather than the two resolved factors.

338

339

As shown in **Fig.5**, compared with PMF results, the proportions of HOA (7%) and COA (11%) obtained by source apportionment with ME-2 have significantly decreased to the expected value during the winter observation (Huang et al., 2020; Xu et al., 2020). As expected, other POA contributions were identified in the highly polluted season, correlated well with $C_2H_4O_2^+$ and $C_{10}H_8^+$, which are well-known fragments from

343 biomass burning and coal combustion emissions (**Fig.5, Fig.S17 and Table S22**) (Alfarra et al., 2007; Duan
344 et al., 2020; Hu et al., 2016a; Lee et al., 2010). The diurnal patterns of HOA_PMF were consistent with
345 HOA_ME-2 during the winter observation, presenting low concentration during the daytime and high
346 concentration at nighttime, likely due to the combined influence of boundary layer height and emissions from
347 diesel vehicles during the nighttime. The temporal variation of two HOA factors showed a high correlation
348 with NO_x (Pearson $r > 0.7$), suggesting two HOA factors are associated with vehicle emissions. Some
349 variabilities existed between the diurnal cycle of COA_PMF and COA_ME-2. However, COA_ME-2
350 correlated better with C₆H₁₀O⁺ than COA_PMF, which was considered a fragment tracer mainly from cooking
351 emissions (Ge et al., 2012; Hu et al., 2016a; Sun et al., 2011; Xu et al., 2016). For SOA factors, the sum of
352 cooking SOA and vehicle LO-SOA had a high correlation with nitrate (Pearson $r = 0.84$; **Fig.S17 and Table**
353 **S22**) and fragments of low-oxidizing substances (C₂H₃O⁺; Pearson $r = 0.95$). In addition, we noticed that the
354 vehicle SOA analyzed by ME-2 exhibited consistency with the diurnal variation of nitrate, especially the
355 reasonable morning peak (~09:00) retained, implying that vehicle SOA is well separated by using ME-2 in
356 winter. MO-OOA resolved via ME-2 was characterized by prominent signal at m/z 28 and m/z 44, consistent
357 with those in OOA identified by using PMF and in other studies (Duan et al., 2020; Kim et al., 2017).
358 Meanwhile, there was a strong correlation between MO-OOA time series and sulfate (Pearson $r = 0.93$), which
359 was representative of regional aging species. Unfortunately, the SOA factor corresponding to other-POA
360 (likely biomass burning OA) has not been resolved. Some studies have been found that OA emitted by biomass
361 burning will be rapidly oxidized in the ambient atmosphere, and the BBOA in the fresh plume is mostly aged
362 OA (Zhou et al., 2017). When the aged biomass burning OA is further oxidized, it is difficult to be identified
363 the biomass burning SOA from mixed within OOA without constraining its SOA factor. Overall, ME-2 source
364 analysis with the input of four source spectra profiles significantly improved the OA source apportionment
365 during the wintertime. In comparing the ME-2 analysis results with only two POA factors constraining to that

of the four factors constraining, the diurnal variations of HOA and COA obtained by constraining two primary sources were more consistent with those of the ME-2 constraint four-factor than PMF. However, OOA and POA were weakly separated, and the diurnal patterns of OOA were correlated with the case for the peak of other-POA during the evening (20:00~21:00) (Fig.S18-S19). These phenomena imply that the SOA factor constraint can be more environmentally meaningful factors to a certain extent.

For the source apportionment in summer with high oxidation conditions (Fig.S20), the fraction of COA reduced from 21% (PMF result) to 12% (ME-2 result). Moreover, the diurnal patterns of ME-2 SOA factors present more reasonable than PMF SOA factors. For example, the MO-OOA obtained based on ME-2 analysis was in good agreement with the diurnal variation of O_x in summer. The Pearson r between MO-OOA_ME-2 and CO_2^+ (m/z 44), a marker of SOA was 0.95, higher than that of MO-OOA_PMF (0.79), which better reflects the characteristics of the MO-OOA factor in ME-2 (Fig.S21 and Table S23). In general, the accurate source apportionment results have significantly indicated that the reliability source profiles of the primary and secondary of cooking and vehicles obtained in our study can be used as constraints for source apportionment of OA with ME-2 in various primary emissions or high oxidation conditions.

4. Limitations and future work

POA emissions, and SOA formation in Go: PAM reactor from urban cooking and vehicular sources were explored. The aged COA had higher hydrocarbon ions than aged HOA in mass spectra. The spectra profiles of urban cooking and vehicular sources derived from the lab simulation were performed as constraints in ME-2 model. The OA source apportionment using ME-2 compared with unconstrained PMF based on the HR OA datasets in Shanghai validated the reasonable of the primary and secondary source profiles of cooking and vehicles. It is noted that the vehicle experiments were solely conducted under a single engine with gasoline, and the cooking experiment only related to limited cooking styles. The variations of VOCs in diesel and gasoline vehicle emissions may lead to differences in the SOA characteristics (Wang et al., 2020). The POA

389 and gas-phase precursor emitted from another cooking style - meat charbroiling can also form a large amount
390 of SOA after photochemical oxidation (Kaltsonoudis et al., 2017). More work needs to be done to explore the
391 POA and SOA mass spectrometric characteristics of emissions from vehicles and cooking sources. In addition,
392 SOA mass spectra were split from aged COA and aged HOA by using the PMF model, and therefore provided
393 limited information on dynamic SOA mass spectra; we suggested that further studies control the oxidation
394 conditions to obtain a set of dynamic pure SOA spectral profile. Especially, the absence of primary HOA due
395 to low emissions of engine, and the inability to separate vehicle PMF POA from aged HOA in the PMF analysis
396 were major limitations of this study. In addition to obtaining pure vehicle POA through source experiments,
397 further work can apply ME-2 model for constraining pure SOA profiles from experimental datasets to obtain
398 the vehicle POA profiles. Constraining many SOA factors could be over-constraining the ME-2 runs, which
399 leads to factor mixing and reduces the number of factors. Therefore, SOA source spectra can only be
400 appropriately and reasonably limited in ME-2 model. Besides, measurements of accurate tracers for all factors
401 that resolved by PMF or ME-2 model should be conducted in future work to improve source apportionment
402 verification. For example, we had to combine vehicle LO-SOA and cooking SOA as LO-OOA due to the lack
403 of the measurement tracers for vehicle and cooking SOA factor, and then we analyzed the time series-
404 correlation of LO-OOA with nitrate and other tracer ions. Due to the limitation of Go: PAM, dilution and high
405 concentration of OH radicals without other inorganic aerosol seeds were adopted to measure and simulate
406 atmospheric aging of aerosols. Thus, the possible atmospheric transformations and the reaction pathway are
407 affected. In the future, it is still necessary to take further researches, for instance, use a quasi-atmospheric
408 aerosol evolution study (QUALITY) chamber (Guo et al., 2020) to study the SOA formation under different
409 actual oxidation conditions, like high/low NO_x and so forth. Moreover, ambient datasets obtained from
410 different sites and seasons need to be analyzed to validate the application of POA and SOA profiles of cooking
411 and vehicles in this study, noting selecting a loose constraint via a value in SOA factors due to their high

412 variability. Our research found that SOA from the urban cooking and vehicular sources contributed 19% and
 413 35% of OA in the wintertime and summertime of Shanghai, implying the need to develop control measures to
 414 reduce emissions from cooking and vehicular sources in the future.

415
 416 **Nomenclature table**

Abbreviations	Description
OA	organic aerosol
POA	primary organic aerosol
SOA	secondary organic aerosol
HOA	hydrocarbon-like organic aerosol; associated with vehicle-related emissions in urban
COA	cooking organic aerosol
LO-OOA	low oxygenated organic aerosol
MO-OOA	more oxygenated organic aerosol
PMF	positive matrix factorization
ME-2	a multilinear engine
HR-ToF-AMS	high-resolution time-of-flight aerosol mass spectrometer
SMPS	scanning mobility particle sizers
Go: PAM	Gothenburg Potential Aerosol Mass reactor
VOCs	volatile organic compounds
SVOCs	semi-volatile organic compounds
IVOCs	intermediate volatile organic compounds
O-VOCs	oxygenated volatile organic compounds
$f_{28, 29, 41, 43, \dots}$	fraction of m/z 28, 29, 41, 43... in total organic aerosol
aged HOA	organic aerosols oxidized by Potential Aerosol Mass reactor in vehicle experiments
aged COA	organic aerosols oxidized by Potential Aerosol Mass reactor in cooking experiments
LO-SOA	low oxidized vehicle secondary organic aerosol
MO-SOA	more oxidized vehicle secondary organic aerosol

417
 418 **Supporting information**

419 Schematic depiction of the simulation and measurement system (Figure S1); Details of the mass spectra of
 420 aged HOA and aged COA (Figures S2-S5; Table S5-S8); Van Krevelen diagram of POA, aged COA, and aged
 421 HOA (Figure S6); The choice for the PMF and ME-2 analysis (Figure S7-S10; Table S9-S10; Figure S13-S14;

Table S20-S21); ME-2 source analysis during the summer observation in Shanghai (Figure S19); The time-series correlations of factors with external tracers (Figure S17-S18, S21; Table S22-S23); Experimental parameters (Table S1-S3); Mass spectra similarity analysis between mass spectra of ambient factor and mass spectral profiles for vehicle and cooking (Table S15-S19; Figure S11).

Data availability. The data provided in this paper can be obtained from the author upon request (songguo@pku.edu.cn).

Author contribution. Wenfei Zhu, Zirui Zhang, Hui Wang, Ying Yu, Zheng Chen, Ruizhe Shen, Rui Tan, Kai Song, Kefan Liu, Rongzhi Tang, Yi Liu, Yuanju Li, Wenbin Zhang, and Zhou Zhang conducted the experiments. Wenfei Zhu, Zirui Zhang, Song Guo, and Min Hu analyzed the data. Shengrong Lou, Shijin Shuai, Hongming Xu, Shuangde Li, Yunfa Chen, Francesco Canonaco, and Andre. S. H. Prévôt reviewed and commented on the paper. Wenfei Zhu and Song Guo wrote the paper.

Competing interests. The authors declare no competing financial interest.

Acknowledgments. This research was supported by the National Natural Science Foundation of China (51636003, 41977179, 91844301), Beijing Municipal Science and Technology Commission (Z201100008220011), the Natural Science Foundation of Beijing (8192022), the fellowship of China Postdoctoral Science Foundation (2020M680242), and the Open Research Fund of State Key Laboratory of Multiphase Complex Systems (No. MPCS-2021-D-12).

References

- Alfarra, M.R., Prevot, A.S.H., Szidat, S., Sandradewi, J., Weimer, S., Lanz, V.A., Schreiber, D., Mohr, M., Baltensperger, U., 2007. Identification of the mass spectral signature of organic aerosols from wood burning emissions. *Environmental Science & Technology* 41, 5770-5777.
- Budisulistiorini, S.H., Canagaratna, M.R., Croteau, P.L., Marth, W.J., Baumann, K., Edgerton, E.S., Shaw, S.L., Knipping, E.M., Worsnop, D.R., Jayne, J.T., Gold, A., Surratt, J.D., 2013. Real-Time Continuous Characterization of Secondary Organic Aerosol Derived from Isoprene Epoxydiols in Downtown Atlanta, Georgia, Using the Aerodyne Aerosol Chemical Speciation Monitor. *Environmental Science & Technology* 47, 5686-5694.
- Canagaratna, M., Jimenez, J., Kroll, J., Chen, Q., Kessler, S., Massoli, P., Hildebrandt Ruiz, L., Fortner, E., Williams, L., Wilson, K., 2015. Elemental ration measurements of organic compounds using aerosol mass spectrometry: characterization, improved calibration, and implications. *Atmos. Chem. Phys* 15, 253-272.

450 Canagaratna, M.R., Jayne, J.T., Jimenez, J.L., Allan, J.D., Alfarra, M.R., Zhang, Q., Onasch, T.B., Drewnick, F., Coe, H.,
451 Middlebrook, A., Delia, A., Williams, L.R., Trimborn, A.M., Northway, M.J., DeCarlo, P.F., Kolb, C.E., Davidovits, P., Worsnop,
452 D.R., 2007. Chemical and microphysical characterization of ambient aerosols with the aerodyne aerosol mass spectrometer.
453 *Mass Spectrometry Reviews* 26, 185–222.

454 Canonaco, F., Crippa, M., Slowik, J.G., Baltensperger, U., Prevot, A.S.H., 2013. SoFi, an IGOR-based interface for the efficient
455 use of the generalized multiline engine (ME-2) for the source apportionment: ME-2 application to aerosol mass
456 spectrometer data. *Atmospheric Measurement Techniques* 6, 3649–3661.

457 Collier, S., Zhou, S., Kuwayama, T., Forestieri, S., Brady, J., Zhang, M., Kleeman, M., Cappa, C., Bertram, T., Zhang, Q., 2015.
458 Organic PM Emissions from Vehicles: Composition, O/C Ratio, and Dependence on PM Concentration. *Aerosol Science and
459 Technology* 49, 86–97.

460 Crippa, M., Canonaco, F., Lanz, V.A., Aijala, M., Allan, J.D., Carbone, S., Capes, G., Ceburnis, D., Dall'Osto, M., Day, D.A.,
461 DeCarlo, P.F., Ehn, M., Eriksson, A., Freney, E., Hildebrandt Ruiz, L., Hillamo, R., Jimenez, J.L., Junninen, H., Kiendler-Scharr,
462 A., Kortelainen, A.M., Kulmala, M., Laaksonen, A., Mensah, A., Mohr, C., Nemitz, E., O'Dowd, C., Ovadnevaite, J., Pandis, S.N.,
463 Petaja, T., Poulain, L., Saarikoski, S., Sellegri, K., Swietlicki, E., Tiitta, P., Worsnop, D.R., Baltensperger, U., Prevot, A.S.H., 2014.
464 Organic aerosol components derived from 25 AMS data sets across Europe using a consistent ME-2 based source
465 apportionment approach. *Atmospheric Chemistry and Physics* 14, 6159–6176.

466 Duan, J., Huang, R.-J., Li, Y., Chen, Q., Zheng, Y., Chen, Y., Lin, C., Ni, H., Wang, M., Ovadnevaite, J., Ceburnis, D., Chen, C.,
467 Worsnop, D.R., Hoffmann, T., O'Dowd, C., Cao, J., 2020. Summertime and wintertime atmospheric processes of secondary
468 aerosol in Beijing. *Atmospheric Chemistry and Physics* 20, 3793–3807.

469 Elser, M., Huang, R.-J., Wolf, R., Slowik, J.G., Wang, Q., Canonaco, F., Li, G., Bozzetti, C., Daellenbach, K.R., Huang, Y., Zhang,
470 R., Li, Z., Cao, J., Baltensperger, U., El-Haddad, I., Prevot, A.S.H., 2016. New insights into PM_{2.5} chemical composition and
471 sources in two major cities in China during extreme haze events using aerosol mass spectrometry. *Atmospheric Chemistry
472 and Physics* 16, 3207–3225.

473 Ge, X., Li, L., Chen, Y., Chen, H., Wu, D., Wang, J., Xie, X., Ge, S., Ye, Z., Xu, J., 2017. Aerosol characteristics and sources in
474 Yangzhou, China resolved by offline aerosol mass spectrometry and other techniques. *Environmental Pollution* 225, 74–85.

475 Ge, X., Setyan, A., Sun, Y., Zhang, Q., 2012. Primary and secondary organic aerosols in Fresno, California during wintertime:
476 Results from high resolution aerosol mass spectrometry. *Journal of Geophysical Research-Atmospheres* 117.

477 Gentner, D.R., Harley, R.A., Miller, A.M., Goldstein, A.H., 2009. Diurnal and Seasonal Variability of Gasoline-Related Volatile
478 Organic Compound Emissions in Riverside, California. *Environmental Science & Technology* 43, 4247–4252.

479 Guo, S., Hu, M., Guo, Q., Zhang, X., Zheng, M., Zheng, J., Chang, C.C., Schauer, J.J., Zhang, R., 2012. Primary Sources and
480 Secondary Formation of Organic Aerosols in Beijing, China. *Environmental Science & Technology* 46, 9846–9853.

481 Guo, S., Hu, M., Peng, J., Wu, Z., Zamora, M.L., Shang, D., Du, Z., Zheng, J., Fang, X., Tang, R., Wu, Y., Zeng, L., Shuai, S.,
482 Zhang, W., Wang, Y., Ji, Y., Li, Y., Zhang, A.L., Wang, W., Zhang, F., Zhao, J., Gong, X., Wang, C., Molina, M.J., Zhang, R., 2020.
483 Remarkable nucleation and growth of ultrafine particles from vehicular exhaust. *Proceedings of the National Academy of
484 Sciences of the United States of America* 117, 3427–3432.

485 Guo, S., Hu, M., Zamora, M.L., Peng, J., Shang, D., Zheng, J., Du, Z., Wu, Z., Shao, M., Zeng, L., Molina, M.J., Zhang, R., 2014.
486 Elucidating severe urban haze formation in China. *Proceedings of the National Academy of Sciences of the United States of
487 America* 111, 17373–17378.

488 He, L.Y., Huang, X.F., Xue, L., Hu, M., Lin, Y., Zheng, J., Zhang, R., Zhang, Y.H., 2011. Submicron aerosol analysis and organic
489 source apportionment in an urban atmosphere in Pearl River Delta of China using high-resolution aerosol mass
490 spectrometry. *Journal of Geophysical Research Atmospheres* 116, -.

491 He, L.Y., Lin, Y., Huang, X.F., Guo, S., Xue, L., Su, Q., Hu, M., Luan, S.J., Zhang, Y.H., 2010. Characterization of high-resolution
492 aerosol mass spectra of primary organic aerosol emissions from Chinese cooking and biomass burning. *Atmospheric
493 Chemistry and Physics* 10, 11535–11543.

494 Hu, W., Hu, M., Hu, W., Jimenez, J.L., Yuan, B., Chen, W., Wang, M., Wu, Y., Chen, C., Wang, Z., 2016a. Chemical composition,
495 sources, and aging process of submicron aerosols in Beijing: Contrast between summer and winter. *Journal of Geophysical*
496 *Research Atmospheres* 121, 1955-1977.

497 Hu, W., Hu, M., Hu, W.W., Zheng, J., Chen, C., Wu, Y., Guo, S., 2017. Seasonal variations in high time-resolved chemical
498 compositions, sources, and evolution of atmospheric submicron aerosols in the megacity Beijing. *Atmospheric Chemistry &*
499 *Physics* 17, 9979-10000.

500 Hu, W., Palm, B.B., Day, D.A., Campuzano-Jost, P., Krechmer, J.E., Peng, Z., de Sa, S.S., Martin, S.T., Alexander, M.L., Baumann,
501 K., Hacker, L., Kiendler-Scharr, A., Koss, A.R., de Gouw, J.A., Goldstein, A.H., Seco, R., Sjostedt, S.J., Park, J.-H., Guenther, A.B.,
502 Kim, S., Canonaco, F., Prevot, A.S.H., Brune, W.H., Jimenez, J.L., 2016b. Volatility and lifetime against OH heterogeneous
503 reaction of ambient isoprene-epoxydiols-derived secondary organic aerosol (IEPOX-SOA). *Atmospheric Chemistry and*
504 *Physics* 16, 11563-11580.

505 Huang, R.-J., He, Y., Duan, J., Li, Y., Chen, Q., Zheng, Y., Chen, Y., Hu, W., Lin, C., Ni, H., Dai, W., Cao, J., Wu, Y., Zhang, R., Xu,
506 W., Ovadnevaite, J., Ceburnis, D., Hoffmann, T., O'Dowd, C.D., 2020. Contrasting sources and processes of particulate species
507 in haze days with low and high relative humidity in wintertime Beijing. *Atmospheric Chemistry and Physics* 20, 9101-9114.

508 Huang, X.F., He, L.Y., Hu, M., Canagaratna, M.R., Kroll, J.H., Ng, N.L., Zhang, Y.H., Lin, Y., Xue, L., Sun, T.L., 2011.
509 Characterization of submicron aerosols at a rural site in Pearl River Delta of China using an Aerodyne High-Resolution
510 Aerosol Mass Spectrometer. *Atmospheric Chemistry & Physics* 11, 1865-1877.

511 Kaltsonoudis, C., Kostenidou, E., Louvaris, E., Psichoudaki, M., Tsiligiannis, E., Florou, K., Liangou, A., Pandis, S.N., 2017.
512 Characterization of fresh and aged organic aerosol emissions from meat charbroiling. *Atmospheric Chemistry and Physics*
513 17, 7143-7155.

514 Katragadda, H.R., Fullana, A., Sidhu, S., Carbonell-Barrachina, A.A., 2010. Emissions of volatile aldehydes from heated
515 cooking oils. *Food Chemistry* 120, 59-65.

516 Kim, H., Zhang, Q., Bae, G.-N., Kim, J.Y., Lee, S.B., 2017. Sources and atmospheric processing of winter aerosols in Seoul,
517 Korea: insights from real-time measurements using a high-resolution aerosol mass spectrometer. *Atmospheric Chemistry*
518 *and Physics* 17, 2009-2033.

519 Klein, F., Platt, S.M., Farren, N.J., Detournay, A., Bruns, E.A., Bozzetti, C., Daellenbach, K.R., Kilic, D., Kumar, N.K., Pieber, S.M.,
520 Slowik, J.G., Temime-Roussel, B., Marchand, N., Hamilton, J.F., Baltensperger, U., Prevot, A.S.H., El Haddad, I., 2016.
521 Characterization of Gas-Phase Organics Using Proton Transfer Reaction Time-of-Flight Mass Spectrometry: Cooking
522 Emissions. *Environmental Science & Technology* 50, 1243-1250.

523 Kostenidou, E., Lee, B.-H., Engelhart, G.J., Pierce, J.R., Pandis, S.N., 2009. Mass Spectra Deconvolution of Low, Medium, and
524 High Volatility Biogenic Secondary Organic Aerosol. *Environmental Science & Technology* 43, 4884-4889.

525 Kroll, J.H., Smith, J.D., Worsnop, D.R., Wilson, K.R., 2012. Characterisation of lightly oxidised organic aerosol formed from
526 the photochemical aging of diesel exhaust particles. *Environmental Chemistry* 9, 211-220.

527 Lee, T., Sullivan, A.P., Mack, L., Jimenez, J.L., Kreidenweis, S.M., Onasch, T.B., Worsnop, D.R., Malm, W., Wold, C.E., Hao, W.M.,
528 Collett, J.L., Jr., 2010. Chemical Smoke Marker Emissions During Flaming and Smoldering Phases of Laboratory Open Burning
529 of Wildland Fuels. *Aerosol Science and Technology* 44, I-V.

530 Li, J., Liu, Q., Li, Y., Liu, T., Huang, D., Zheng, J., Zhu, W., Hu, M., Wu, Y., Lou, S., Hallquist, A.M., Hallquist, M., Chan, C.K.,
531 Canonaco, F., Prevot, A.S.H., Fung, J.C.H., Lau, A.K.H., Yu, J.Z., 2019. Characterization of Aerosol Aging Potentials at Suburban
532 Sites in Northern and Southern China Utilizing a Potential Aerosol Mass (Go:PAM) Reactor and an Aerosol Mass
533 Spectrometer. *Journal of Geophysical Research-Atmospheres* 124, 5629-5649.

534 Li, Y.J., Sun, Y., Zhang, Q., Li, X., Li, M., Zhou, Z., Chan, C.K., 2017. Real-time chemical characterization of atmospheric
535 particulate matter in China: A review. *Atmospheric Environment* 158, 270-304.

536 Liu, T., Li, Z., Chan, M., Chan, C.K., 2017. Formation of secondary organic aerosols from gas-phase emissions of heated
537 cooking oils. *Atmospheric Chemistry and Physics* 17, 7333-7344.

538 Liu, T., Wang, Z., Wang, X., Chan, C.K., 2018. Primary and secondary organic aerosol from heated cooking oil emissions.
539 *Atmospheric Chemistry and Physics* 18, 11363-11374.

540 Louvaris, E.E., Karnezi, E., Kostenidou, E., Kaltsonoudis, C., Pandis, S.N., 2017. Estimation of the volatility distribution of
541 organic aerosol combining thermodenuder and isothermal dilution measurements. *Atmospheric Measurement Techniques*
542 10, 3909-3918.

543 Mohr, C., DeCarlo, P.F., Heringa, M.F., Chirico, R., Slowik, J.G., Richter, R., Reche, C., Alastuey, A., Querol, X., Seco, R., Penuelas,
544 J., Jimenez, J.L., Crippa, M., Zimmermann, R., Baltensperger, U., Prevot, A.S.H., 2012. Identification and quantification of
545 organic aerosol from cooking and other sources in Barcelona using aerosol mass spectrometer data. *Atmospheric Chemistry*
546 *and Physics* 12, 1649-1665.

547 Ng, N.L., Canagaratna, M.R., Jimenez, J.L., Zhang, Q., Ulbrich, I.M., Worsnop, D.R., 2011. Real-Time Methods for Estimating
548 Organic Component Mass Concentrations from Aerosol Mass Spectrometer Data. *Environmental Science & Technology* 45,
549 910-916.

550 Paatero, P., 1999. The multilinear engine - A table-driven, least squares program for solving multilinear problems, including
551 the n-way parallel factor analysis model. *Journal of Computational and Graphical Statistics* 8, 854-888.

552 Paatero, P., Hopke, P.K., 2003. Discarding or downweighting high-noise variables in factor analytic models. *Analytica*
553 *Chimica Acta* 490, 277-289.

554 Peng, Z., Day, D.A., Ortega, A.M., Palm, B.B., Hu, W., Stark, H., Li, R., Tsigaridis, K., Brune, W.H., Jimenez, J.L., 2016. Non-OH
555 chemistry in oxidation flow reactors for the study of atmospheric chemistry systematically examined by modeling.
556 *Atmospheric Chemistry and Physics* 16, 4283-4305.

557 Presto, A.A., Gordon, T.D., Robinson, A.L., 2014. Primary to secondary organic aerosol: evolution of organic emissions from
558 mobile combustion sources. *Atmospheric Chemistry and Physics* 14, 5015-5036.

559 Qin, Y.M., Tan, H.B., Li, Y.J., Schurman, M.I., Li, F., Canonaco, F., Prevot, A.S.H., Chan, C.K., 2017. Impacts of traffic emissions
560 on atmospheric particulate nitrate and organics at a downwind site on the periphery of Guangzhou, China. *Atmospheric*
561 *Chemistry and Physics* 17, 10245-10258.

562 Reyes-Villegas, E., Green, D.C., Priestman, M., Canonaco, F., Coe, H., Prevot, A.S.H., Allan, J.D., 2016. Organic aerosol source
563 apportionment in London 2013 with ME-2: exploring the solution space with annual and seasonal analysis. *Atmospheric*
564 *Chemistry and Physics* 16, 15545-15559.

565 Robinson, A.L., Donahue, N.M., Shrivastava, M.K., Weitkamp, E.A., Sage, A.M., Grieshop, A.P., Lane, T.E., Pierce, J.R., Pandis,
566 S.N., 2007. Rethinking organic aerosols: Semivolatile emissions and photochemical aging. *Science* 315, 1259-1262.

567 Schauer, J.J., Kleeman, M.J., Cass, G.R., Simoneit, B.R.T., 2002. Measurement of emissions from air pollution sources. 4. C-1-
568 C-27 organic compounds from cooking with seed oils. *Environmental Science & Technology* 36, 567-575.

569 Sun, J., Zhang, Q., Canagaratna, M.R., Zhang, Y., Ng, N.L., Sun, Y., Jayne, J.T., Zhang, X., Zhang, X., Worsnop, D.R., 2010.
570 Highly time- and size-resolved characterization of submicron aerosol particles in Beijing using an Aerodyne Aerosol Mass
571 Spectrometer. *Atmospheric Environment* 44, 131-140.

572 Sun, Y., Du, W., Fu, P., Wang, Q., Li, J., Ge, X., Zhang, Q., Zhu, C., Ren, L., Xu, W., 2016. Primary and secondary aerosols in
573 Beijing in winter: sources, variations and processes. *Atmospheric Chemistry & Physics* 16, 1-41.

574 Sun, Y., Jiang, Q., Wang, Z., Fu, P., Li, J., Yang, T., Yin, Y., 2014. Investigation of the sources and evolution processes of severe
575 haze pollution in Beijing in January 2013. *Journal of Geophysical Research Atmospheres* 119, 4380-4398.

576 Sun, Y., Xu, W., Zhang, Q., Jiang, Q., Canonaco, F., Prévôt, A.S., Fu, P., Li, J., Jayne, J., Worsnop, D.R., 2018. Source
577 apportionment of organic aerosol from two-year highly time-resolved measurements by an aerosol chemical speciation
578 monitor in Beijing, China. *Atmospheric Chemistry and Physics Discussions*, 1-33.

579 Sun, Y.L., Zhang, Q., Schwab, J.J., Demerjian, K.L., Chen, W.N., Bae, M.S., Hung, H.M., Hogrefe, O., Frank, B., Rattigan, O.V.,
580 Lin, Y.C., 2011. Characterization of the sources and processes of organic and inorganic aerosols in New York city with a
581 high-resolution time-of-flight aerosol mass spectrometer. *Atmospheric Chemistry and Physics* 11, 1581-1602.

582 Tang, R.Z., Lu, Q.Y., Guo, S., Wang, H., Song, K., Yu, Y., Tan, R., Liu, K.F., Shen, R.Z., Chen, S.Y., Zeng, L.M., Jorga, S.D., Zhang,
583 Z., Zhang, W.B., Shuai, S.J., Robinson, A.L., 2021. Measurement report: Distinct emissions and volatility distribution of
584 intermediate-volatility organic compounds from on-road Chinese gasoline vehicles: implication of high secondary organic
585 aerosol formation potential. *Atmospheric Chemistry and Physics* 21, 2569-2583.

586 Ulbrich, I., Canagaratna, M., Zhang, Q., Worsnop, D., Jimenez, J., 2009. Interpretation of organic components from positive
587 matrix factorization of aerosol mass spectrometric data. *Atmospheric Chemistry & Physics* 9.

588 Wang, H., Guo, S., Yu, Y., Shen, R., Zhu, W., Tang, R., Tan, R., Liu, K., Song, K., Zhang, W., Zhang, Z., Shuai, S., Xu, H., Zheng,
589 J., Chen, S., Li, S., Zeng, L., Wu, Z., 2021. Secondary aerosol formation from a Chinese gasoline vehicle: Impacts of fuel (E10,
590 gasoline) and driving conditions (idling, cruising). *The Science of the total environment* 795, 148809-148809.

591 Wang, H., Xiang, Z., Wang, L., Jing, S., Lou, S., Tao, S., Liu, J., Yu, M., Li, L., Lin, L., Chen, Y., Wiedensohler, A., Chen, C., 2018.
592 Emissions of volatile organic compounds (VOCs) from cooking and their speciation: A case study for Shanghai with
593 implications for China. *Science of the Total Environment* 621, 1300-1309.

594 Wang, J., Ge, X., Chen, Y., Shen, Y., Zhang, Q., Sun, Y., Xu, J., Ge, S., Yu, H., Chen, M., 2016. Highly time-resolved urban
595 aerosol characteristics during springtime in Yangtze River Delta, China: insights from soot particle aerosol mass spectrometry.
596 *Atmospheric Chemistry and Physics* 16, 9109-9127.

597 Wang, M., Li, S., Zhu, R., Zhang, R., Zu, L., Wang, Y., Bao, X., 2020. On-road tailpipe emission characteristics and ozone
598 formation potentials of VOCs from gasoline, diesel and liquefied petroleum gas fueled vehicles. *Atmospheric Environment*
599 223.

600 Wang, Y.C., Huang, R.J., Ni, H.Y., Chen, Y., Wang, Q.Y., Li, G.H., Tie, X.X., Shen, Z.X., Huang, Y., Liu, S.X., Dong, W.M., Xue, P.,
601 Frohlich, R., Canonaco, F., Elser, M., Daellenbach, K.R., Bozzetti, C., Haddad, I.E., Prevot, A.S.H., Canagaratna, M.R., Worsnop,
602 D.R., Cao, J.J., 2017. Chemical composition, sources and secondary processes of aerosols in Baoji city of northwest China.
603 *Atmospheric Environment* 158, 128-137.

604 Watne, A.K., Psichoudaki, M., Ljungstrom, E., Le Breton, M., Hallquist, M., Jerksjo, M., Fallgren, H., Jutterstrom, S., Hallquist,
605 A.M., 2018. Fresh and Oxidized Emissions from In-Use Transit Buses Running on Diesel, Biodiesel, and CNG. *Environmental*
606 *Science & Technology* 52, 7720-7728.

607 Xu, J., Shi, J., Zhang, Q., Ge, X., Canonaco, F., Prévôt, A.S., Vonwiller, M., Szidat, S., Ge, J., Ma, J., 2016. Wintertime organic
608 and inorganic aerosols in Lanzhou, China: sources, processes, and comparison with the results during summer. *Atmospheric*
609 *Chemistry and Physics* 16, 14937-14957.

610 Xu, W., Han, T., Wei, D., Wang, Q., Chen, C., Jian, Z., Zhang, Y., Jie, L., Fu, P., Wang, Z., 2017. Effects of Aqueous-phase and
611 Photochemical Processing on Secondary Organic Aerosol Formation and Evolution in Beijing, China. *Environmental Science*
612 *& Technology* 51, 762.

613 Xu, W., He, Y., Qiu, Y., Chen, C., Xie, C., Lei, L., Li, Z., Sun, J., Li, J., Fu, P., Wang, Z., Worsnop, D., Sun, Y., 2020. Mass spectral
614 characterization of primary emissions and implications in source apportionment of organic aerosol. *Atmospheric*
615 *Measurement Techniques* 13, 3205-3219.

616 Ying, Y.A.B., Hui, W.A., A, T.W., Kai, S.A., A, T.T., A, Z.W., C, Y.G., A, H.D., A, S.C., D, L.Z.A.B., 2020. Elucidating the importance
617 of semi-volatile organic compounds to secondary organic aerosol formation at a regional site during the EXPLORE-YRD
618 campaign - ScienceDirect. *Atmospheric Environment*.

619 Yu, Y., Wang, H., Wang, T.T., Song, K., Tan, T.Y., Wan, Z.C., Gao, Y.Q., Dong, H.B., Chen, S.Y., Zeng, L.M., Hu, M., Wang, H.L.,
620 Lou, S.R., Zhu, W.F., Guo, S., 2021. Elucidating the importance of semi-volatile organic compounds to secondary organic
621 aerosol formation at a regional site during the EXPLORE-YRD campaign. *Atmospheric Environment* 246.

622 Zhang, Q., Jimenez, J.L., Canagaratna, M.R., Ulbrich, I.M., Ng, N.L., Worsnop, D.R., Sun, Y., 2011. Understanding atmospheric
623 organic aerosols via factor analysis of aerosol mass spectrometry: a review. *Analytical & Bioanalytical Chemistry* 401, 3045-
624 3067.

625 Zhang, X., Zhang, Y., Sun, J., Yu, Y., Canonaco, F., Prevot, A.S.H., Li, G., 2017a. Chemical characterization of submicron aerosol
626 particles during wintertime in a northwest city of China using an Aerodyne aerosol mass spectrometry. *Environmental*
627 *Pollution* 222, 567-582.

628 Zhang, Y., Tang, L., Sun, Y., Favez, O., Canonaco, F., Albinet, A., Couvidat, F., Liu, D., Jayne, J.T., Wang, Z., Croteau, P.L.,
629 Canagaratna, M.R., Zhou, H.-c., Prevot, A.S.H., Worsnop, D.R., 2017b. Limited formation of isoprene epoxydiols-derived
630 secondary organic aerosol under NO_x-rich environments in Eastern China. *Geophysical Research Letters* 44, 2035-2043.

631 Zhang, Y.J., Tang, L.L., Wang, Z., Yu, H.X., Sun, Y.L., Liu, D., Qin, W., Zhang, H.L., Zhou, H.C., 2014. Insights into characteristics,
632 sources and evolution of submicron aerosols during harvest seasons in Yangtze River Delta (YRD) region, China.
633 *Atmospheric Chemistry & Physics* 14, 9109-9154.

634 Zhang, Z., Zhu, W., Hu, M., Wang, H., Chen, Z., Shen, R., Yu, Y., Tan, R., Guo, S., 2020. Secondary Organic Aerosol from
635 Typical Chinese Domestic Cooking Emissions. *Environmental Science & Technology Letters*.

636 Zhou, S., Collier, S., Jaffe, D.A., Briggs, N.L., Hee, J., Sedlacek, A.J., III, Kleinman, L., Onasch, T.B., Zhang, Q., 2017. Regional
637 influence of wildfires on aerosol chemistry in the western US and insights into atmospheric aging of biomass burning organic
638 aerosol. *Atmospheric Chemistry and Physics* 17, 2477-2493.

639 Zhou, W., Wang, Q., Zhao, X., Xu, W., Chen, C., Du, W., Zhao, J., Canonaco, F., Prevot, A.S.H., Fu, P., Wang, Z., Worsnop, D.R.,
640 Sun, Y., 2018. Characterization and source apportionment of organic aerosol at 260 m on a meteorological tower in Beijing,
641 China. *Atmospheric Chemistry and Physics* 18, 3951-3968.

642 Zhu, Q., Huang, X.-F., Cao, L.-M., Wei, L.-T., Zhang, B., He, L.-Y., Elser, M., Canonaco, F., Slowik, J.G., Bozzetti, C., El-Haddad,
643 I., Prevot, A.S.H., 2018. Improved source apportionment of organic aerosols in complex urban air pollution using the
644 multilinear engine (ME-2). *Atmospheric Measurement Techniques* 11, 1049-1060.

645 Zhu, W., Guo, S., Lou, S., Wang, H., Yu, Y., Xu, W., Liu, Y., Cheng, Z., Huang, X., He, L., Zeng, L., Chen, S., Hu, M., 2021a. A
646 novel algorithm to determine the scattering coefficient of ambient organic aerosols. *Environmental Pollution* 270.

647 Zhu, W., Zhou, M., Cheng, Z., Yan, N., Huang, C., Qiao, L., Wang, H., Liu, Y., Lou, S., Guo, S., 2021b. Seasonal variation of
648 aerosol compositions in Shanghai, China: Insights from particle aerosol mass spectrometer observations. *The Science of the*
649 *total environment* 771, 144948-144948.

650